

Linear and nonlinear optical response of g-C_3N_4-based quantum dots

Jing-Zhi Zhang(张竞之) and Hong Zhang(张红)

Citation: Chin. Phys. B, 2021, 30 (**7**): 077802. DOI: 10.1088/1674-1056/abec2f
Journal homepage: http://cpb.iphy.ac.cn; http://iopscience.iop.org/cpb

What follows is a list of articles you may be interested in

Modulation of the second-harmonic generation in MoS_2 by graphene covering

Chunchun Wu(吴春春), Nianze Shang(尚念泽), Zixun Zhao(赵子荀), Zhihong Zhang(张智宏), Jing Liang(梁晶), Chang Liu(刘畅), Yonggang Zuo(左勇刚), Mingchao Ding(丁铭超), Jinhuan Wang(王金焕), Hao Hong(洪浩), Jie Xiong(熊杰), and Kaihui Liu(刘开辉)

Chin. Phys. B, 2021, 30 (**2**): 027803. DOI: 10.1088/1674-1056/abd77f

Effect of spatially nonlocal versus local optical response of a gold nanorod on modification of the spontaneous emission

Sha-Sha Wen(文莎莎), Meng Tian(田锰), Hong Yang(杨红), Su-Jun Xie(谢素君), Xiao-Yun Wang(王小云), Yun Li(李芸), Jie Liu(刘杰), Jin-Zhang Peng(彭金璋), Ke Deng(邓科), He-Ping Zhao(赵鹤平), and Yong-Gang Huang(黄勇刚)

Chin. Phys. B, 2021, 30 (**2**): 027801. DOI: 10.1088/1674-1056/abc238

Broadband strong optical dichroism in topological Dirac semimetals with Fermi velocity anisotropy

J Lim(林镇杰), K J A Ooi(黄健安), C Zhang(涨潮), L K Ang(洪礼祺), Yee Sin Ang(洪逸欣)

Chin. Phys. B, 2020, 29 (**7**): 077802. DOI: 10.1088/1674-1056/ab928e

Cascaded plasmonic nanorod antenna for large broadband local electric field enhancement

Dou Zhang(张豆), Zhong-Jian Yang(杨中见), Jun He(何军)

Chin. Phys. B, 2019, 28 (**10**): 107802. DOI: 10.1088/1674-1056/ab3f99

Optical response of tunable terahertz plasmon in a grating-gated graphene transistor

Bo Yan(闫博), Jingyue Fang(方靖岳), Shiqiao Qin(秦石乔), Yongtao Liu(刘永涛), Li Chen(陈力), Shuang Chen(陈爽), Renbing Li(李仁兵), Zhen Han(韩震)

Chin. Phys. B, 2017, 26 (**9**): 097802. DOI: 10.1088/1674-1056/26/9/097802

Linear and nonlinear optical response of g-C_3N_4-based quantum dots*

Jing-Zhi Zhang(张竞之)[1] and Hong Zhang(张红)[1,2,†]

[1] College of Physics, Sichuan University, Chengdu 610065, China

[2] Key Laboratory of High Energy Density Physics and Technology of Ministry of Education, Sichuan University, Chengdu 610065, China

(Received 2 February 2021; revised manuscript received 28 February 2021; accepted manuscript online 5 March 2021)

Graphite carbon nitride (g-C_3N_4) attracts wide-ranging research interest due to its extraordinary physicochemical properties and promising applications ranging from heterogeneous catalysis to fuel cells. In this work, we design different g-C_3N_4-based quantum dots (gCNQDs), carry out a systematic study of optical properties, and elucidate the shape selectivity, composite nanostructure, and outfield effect. In particular, composites of gCNQDs and metal nanochains present excellent optical response, making it applicable to bioimaging, nano-plasma devices, and metalloenzyme in infrared light related fields. Besides, QDs which original bridging nitrogen atoms are replaced by amino (–NH_2), hydroxyl (–OH), and methyl (–CH_3) functional groups respectively, have excellent spectral selectivity in the deep ultraviolet region. More interestingly, in the study of the laser interaction with materials, the gCNQDs exhibit extremely high stability and light corrosion resistance. Phase transition from insulation to metal is observed under the critical condition of about 5 eV intensity or 337 nm wavelength. All provided theoretical support for designs and applications in g-C_3N_4 quantum devices.

Keywords: graphite carbon nitride, optical response, ultra-fast laser, plasmon

PACS: 78.67.Hc, 78.67.–n, 73.20.Mf, 79.20.Ds **DOI:** 10.1088/1674-1056/abec2f

1. Introduction

Graphitic carbon nitride (g-C_3N_4) is a dazzling star in the field of semiconductor photocatalysis technology, which has become one of the most attractive research fields for removing organic pollutants and converting solar energy.[1,2] As a metal-free catalyst, g-C_3N_4 has been widely used in photo-splitting water to produce hydrogen,[3,4] photo-degrading organic pollutants,[5,6] and photo-catalytic CO_2 reduction.[7,8] It is the most stable allotrope among various carbonitrides under ambient conditions, with unique optical and electronic properties, high thermal and chemical stability, and low synthesis cost.[9–12] However, wide band gap ~ 2.7 eV, small specific surface area, and high photo-generated hole recombination rate limit the application of g-C_3N_4.[13]

With the deepening of theories and experiments, g-C_3N_4 has gradually been applied to the field of optoelectronics as diodes, lithium batteries, storages, and photodetectors. Today with increasingly higher requirements for integration, to improve light utilization, theoretical research on g-C_3N_4-based quantum dots (QDs) is far from enough, which arouses our great interest. g-C_3N_4 is generally synthesized by thermal condensation of nitrogen-rich precursors such as cyanamide, dicyandiamide, and melamine.[14] Yang *et al.*[15] have synthesized ultra-thin g-C_3N_4 nanosheets with a thickness of about 2 nm. Research has focused on the modification of g-C_3N_4 to obtain better performance.[16–18] The specific surface area of g-C_3N_4 with a layered structure similar to graphite can be increased to as high as 2500 $m^2 \cdot g^{-1}$ theoretically.[19] In addition, the morphology modulation of g-C_3N_4 has been demonstrated as a successful method to endow it with large specific surface areas, abundant reaction sites for promoting light-harvesting, charge separation and transfer, and mass diffusion, all of which enhance the photocatalytic performance. For example, Zhang *et al.*[20] have fabricated g-C_3N_4 with ordered mesopores and cylindrical channels to have a surface area up to 517 $m^2 \cdot g^{-1}$. At the atomic level, reasonable simulations and basic calculations help to design and synthesis g-C_3N_4.

To improve light energy utilization of g-C_3N_4, this paper combines band gap engineering and other modification strategies to design QDs based on g-C_3N_4, and calculates the electronic and optical properties of each composite through first-principles theory. We first explore the optical response of QDs under basic control methods such as polarization direction, the number of layers and size, thus proves the adjustability of band gap and reveals the law of light absorption. Next, the use of precious metal chain coupling, functional group modification, etc. attempts to expand the visible light absorption of the g-C_3N_4 composites.

2. Computational details

Calculations are performed based on *ab initio* density functional theory (DFT) as implemented in the CASTEP[21]

*Project supported by the National Key R&D Program of China (Grant No. 2017YFA0303600), the National Natural Science Foundation of China (Grant No. 11974253), and Science Speciality Program of Sichuan University (Grant No. 2020SCUNL210).

†Corresponding author. E-mail: hongzhang@scu.edu.cn

© 2021 Chinese Physical Society and IOP Publishing Ltd

and OCTOPUS[22] codes. First, geometries are optimized by CASTEP using the gradient approximation (GGA) expressed by the Perdew–Burke–Ernzerhof (PBE)[23] function for the exchange–correlation. The energy band and density of states are calculated using HSEO6 hybrid functional.

The central tenet is that all physical properties of an interacting many-electron system can be determined from its time-dependent density.[24,25] We numerically propagate Eq. (1) in real time and real space using the OCTOPUS code. Carbon, nitrogen, hydrogen, copper, silver, and gold atoms are described by the Hartwigsen–Goedecker–Hutter pseudopotentials. We perform calculations in a 7 Å radius spherical box and discretize the problem on a Cartesian grid with spacing 0.2 Å. In real-time propagation, an approximated enforced time-reversal symmetry (AETRS) algorithm is used to approximate the evolutionary operator. The motion equation of the system is the time-dependent Kohn–Sham equation

$$\mathrm{i}\frac{\partial}{\partial t}\psi_i(r,t) = \left[-\frac{\nabla^2}{2} + V_{\mathrm{KS}}(\boldsymbol{r},t)\right]\psi_i(r,t), \tag{1}$$

that the electron wave function $\psi_i(r,t)$ obeys, evolved for typically 6000 steps with a time step of $\Delta t = 0.003\hbar/\mathrm{eV}$. The system is excited by a functional pulse that describes the perturbation of the total density of the system to obtain a linear optical absorption spectrum in a particular direction. At time $t = 0$, all the wave functions have an instantaneous phase shift

$$\psi_i(\boldsymbol{r},\delta t) = \exp(\mathrm{i}\boldsymbol{k}_0 z)\,\psi_i(\boldsymbol{r},0), \tag{2}$$

where $\boldsymbol{k}_0$ is the perturbation of the external field momentum along the z direction. Then, the time-dependent dipole moment $\boldsymbol{d}(t)$ can be obtained from the time evolution of the Kohn–Sham wave function. The dynamic polarizability $\alpha(\omega)$ is derived by using the Fourier transform of the dipole moment and the induced charge density distribution is extracted accordingly. The absorption spectrum is expressed as a dipole intensity function $S(\omega)$, and its relation with polarizability is $S(\omega) = (2\omega/\pi)\,\mathrm{Im}\alpha(\omega)$.

We simulate the laser–atom interaction with the dipole approximation using an external potential defined as

$$f(x,y,z)\cos(\omega t + \phi(t))\,g(t), \tag{3}$$

$$g(t) = G_0 \exp\left[-(t-t_0)^2/2\tau_0^2\right], \tag{4}$$

where $f(x,y,z)$ is defined by a field type and polarization or a scalar potential, cosine controls the waveform, ω controls the frequency, and ϕ is the time-dependent phase. The $g(t)$ function centered around t_0 describes the waveform of the ultrafast laser. For the time evolution, we use a time step of $0.003\hbar/\mathrm{eV} \approx 0.0020$ fs.

3. Results and discussion

3.1. Geometry and electronic structure of the monolayer g-C_3N_4

The pristine g-C_3N_4 structure is a two-dimensional framework of tri-s-triazine (tri-ring of C_6N_7) subunits linked by tertiary amines. The optimized monolayer g-C_3N_4 reference structure is displayed in Fig. 1, with lattice constants of $a_1 = a_2 = 6.95$ Å. The calculation results of the electronic properties (see Fig. 2), containing the band structure and density of states, show that monolayer g-C_3N_4 is a large direct-gap semiconductor with a bandgap of 2.925 eV. The energy distribution of the conduction band is between 2.4 eV and 10.4 eV, mainly including two density peaks of states, which are mostly contributed by the p orbitals of nitrogen and carbon atoms. The valence band near the Fermi level is mainly contributed by the p orbitals of nitrogen atoms. It corresponds to the fact that in photocatalysis, nitrogen atoms provide oxidation and reduction active sites, while carbon atoms provide reduction active sites.[26]

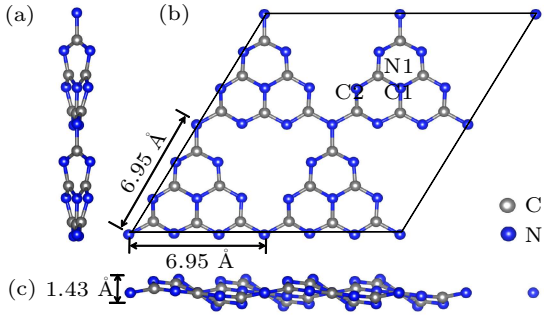


Fig. 1. (a) Side, (b) top, and (c) front views of optimized monolayer g-C_3N_4. Silver and blue atoms sand for carbon and nitrogen, respectively.

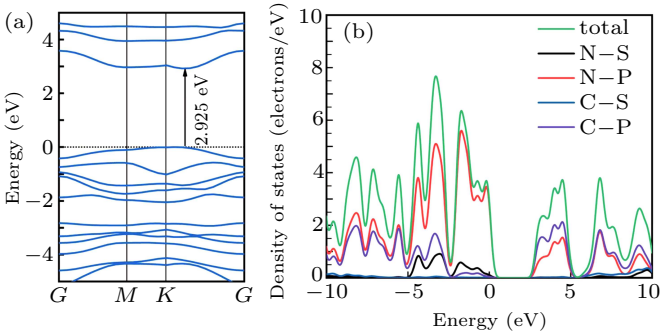


Fig. 2. (a) Electronic band structure, (b) density of states (DOS) and partial densities of states(PDOSs) of monolayer g-C_3N_4.

3.2. Linear optical response of g-C_3N_4 quantum dots

3.2.1. Adjustment of polarization direction, number of layers, and size

The properties of nanostructures and macroscopic materials are completely different due to quantum confinement effects. In order to design kinds of gCNQDs, we selected the periodic minimum unit structure of g-C_3N_4 containing 10 nitrogen atoms and 6 carbon atoms. Because it is like but not

synthetic precursor melem unit. The dangling bonds at the edges are passivated by hydrogen atoms, as shown in the inset in Fig. 3(a). Figure 3(a) displays the results of optical responses when perturbation pulses with different polarization directions are applied to gCNQDs. It shows that gCNQDs have high responsivity in the ultraviolet region, revealing its application potential in the field of thin-film solar cells, photosensitive detectors, optical switches, and photoelectric converters. When the angle of the excitation direction relative to the X axis is between -30° and 90°, the difference in the absorption spectrum is mainly reflected in the highest peak (approximately at 4.8 eV) intensity, where 0° (parallel to the X axis) has the highest photoresponse. Besides, we find effective optical transitions for the first pair of valence and conduction bands (approximately at 3 eV) in low-energy regions that are magnified in the inset. Although the difference is subtle, we find that -30° and 60° have better performance.

To explore the mechanism, we analyze the planar discrete Fourier transform of the induced-charge density distribution at respective energy resonance points displayed in Fig. 3(b). The distance from the upper surface of gCNQDs to the induced density plane is 0.9 Å. Most of the induced electrons and holes are distributed on the edges of the nanostructures, with antisymmetric characteristics, presenting a dipole distribution, which is an antiphase double dipole mode of plasmons excitation. Because of the extended π bond in g-C_3N_4, under the external field induction and electronic screening, the phenomenon of electron aggregation excitation and long-range charge transfer occur. Comparing the induced-charge at the intrinsic absorption peak, the electron–hole density at 0 excitation direction is concentrated with more obvious bilateral symmetry, followed by 60°. This is reflected in their stronger peaks in Fig. 3(a), revealing the advantage of plasmon resonance when excited parallel to the edge of the structure due to the long-distance transfer of electrons to the terminal nitrogen atoms. However, the regularity differs in the low energy region (2 eV–4 eV), which is affected by the original wave configuration of g-C_3N_4 according to our conjecture.

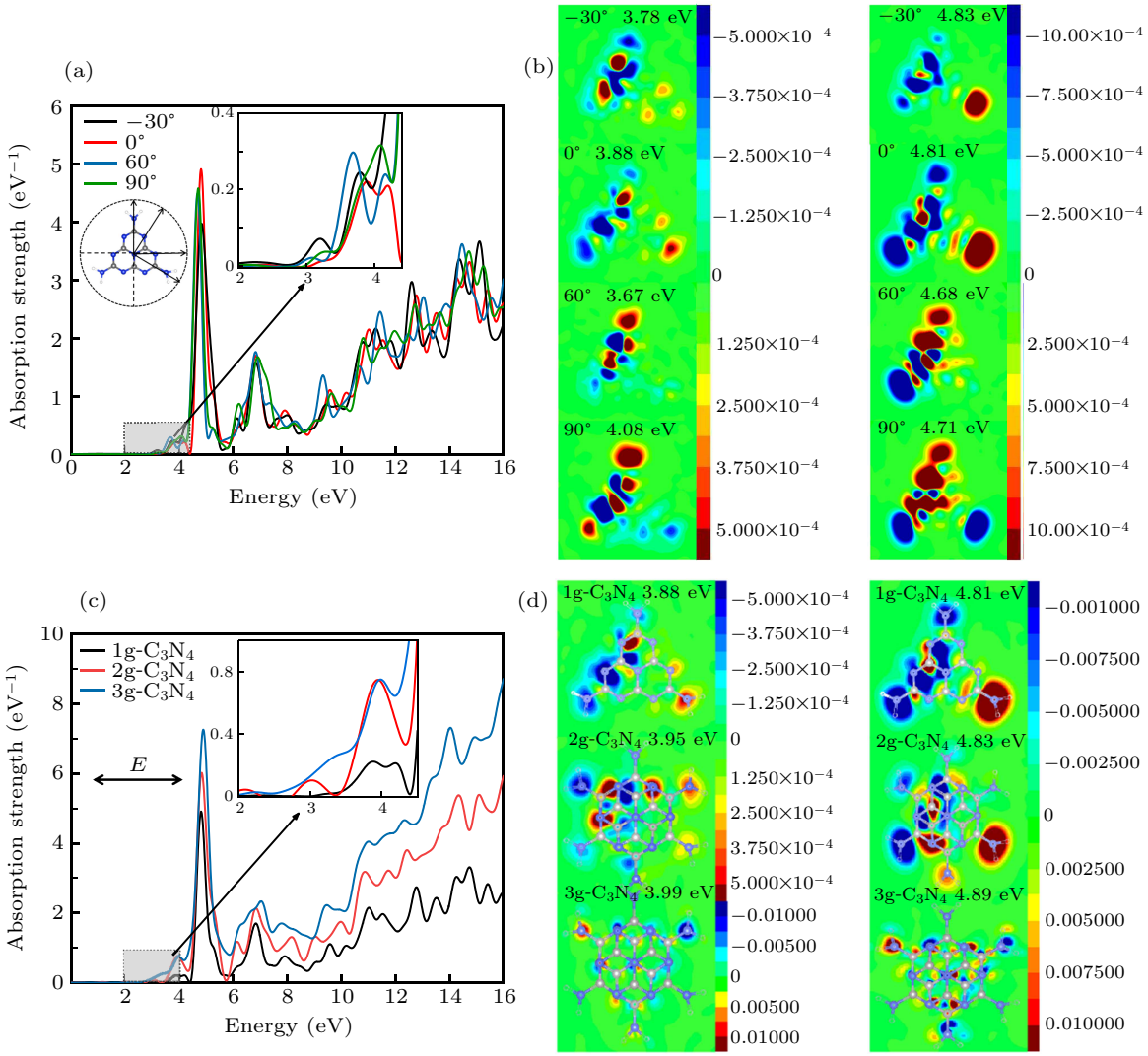


Fig. 3. Optical absorption of (a) g-C_3N_4 as a function of the polarization angle relative to the X axis ($\theta = -30^\circ$, 0°, 60°, 90°) and (b) monolayer gCNQDs (1g-C_3N_4), bilayer gCNQDs (2g-C_3N_4), and trilayer gCNQDs (3g-C_3N_4). Panels (b) and (d) are Fourier transformations of the induced-charge density distribution at energy resonance points.

Figure 3(c) shows the light absorption of few-layer gCNQDs stacked in ABA with pulses in the X direction, corresponding to 1g-C_3N_4 (monolayer), 2g-C_3N_4 (bilayer), and 3g-C_3N_4 (trilayer). The layer spacing is 3.3 Å.[27] As the number of layers increases, the peak value increases nonlinearly. It can be attributed to the formation of an electric field due to the excited state charge transfer caused by light absorption, which impairs the dipole response of the adjacent layer. The corresponding energy gap decreases as the number of layers increases shown in the enlarged part of Fig. 3(c). As seen in Fig. 3(d), the induced charge density distributions at two energy resonance points of different layers have dipole oscillation characteristics, although the charge distribution in the high-energy region is more scattered. Especially for the electron–hole pairs of 3g-C_3N_4 at 3.99 eV and 4.89 eV, we point out that there is a high energy mode of plasmons excitation[28–30] different from long-range charge transfer. It confirms that the interlayer interaction weakens the double dipole response.

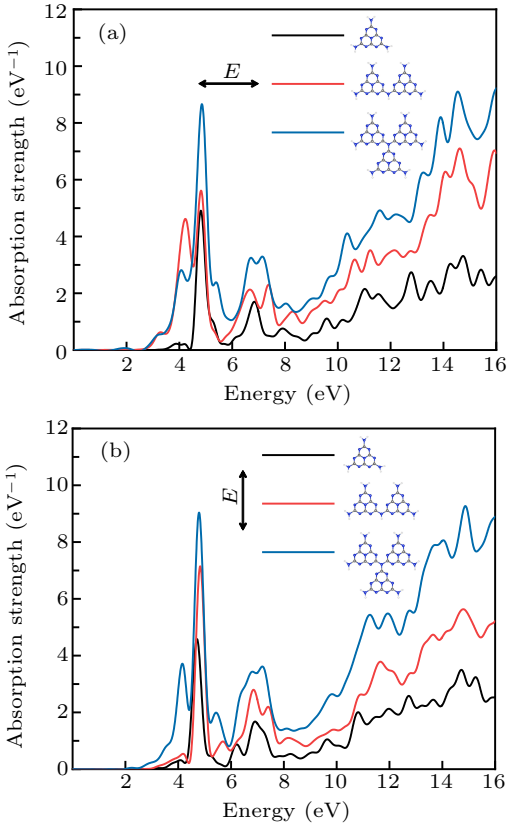


Fig. 4. Optical absorption of three kinds of gCNQDs when the impulse excitation polarized along the X-axis (a) and Y-axis (b), respectively. Structural diagrams are displayed in legends.

For comparison, we add two quantum dots polymerized in perpendicular directions shown in legends of Fig. 4. Spectra indicate that the width of the quantum dots increases along the polarization direction, the absorption peak of the low-energy region is red-shifted and the intensity increases, while the widening of the size along the vertical polarization direction only increases the absorption intensity. It is related to the in-plane electron confinement effect of the small two-dimensional nanostructure.[31] Quantum size effect affects dipole response. Besides, similar to the result of layer number control, the size widening gives rise to a decrease in the band gap along the polarization direction, as low as 2 eV. The widening of the band gap of gCNQDs indicates that the dielectric is enhanced.

3.2.2. Metal/gCNQDs composites

Recently, the exploration of g-C_3N_4-based composite photocatalysts has attracted widespread attention. In a tentative work, we select three kinds of metal nanochains as representatives to compound with gCNQDs. Metal/gCNQDs composites are expected to be widely used as a photosensitizer *in vivo*.[32] The gCNQDs is inserted into metal nanochains composed of 8 copper, silver, and gold atoms respectively along the X-axis direction, and the interatomic distances of these metal atoms are taken as experimental values of 2.55 Å, 2.89 Å, and 2.89 Å, respectively. The distance between the terminal metal atom and its nearest hydrogen atom is 2.89 Å as well.[33] We denote these composites as Cu/g-C_3N_4, Ag/g-C_3N_4, and Au/g-C_3N_4. The impulse excites along the X-axis.

Figures 5(a)–5(c) present the absorption spectrum of the composites (Cu/g-C_3N_4, Ag/g-C_3N_4, and Au/g-C_3N_4), the separate gCNQDs (g-C_3N_4), and the isolated metal nanowires (Cu, Ag, and Au). Surprisingly, strong significant absorption peaks with higher intrinsic intensity and red-shift energy appear in the visible light region, compared with metal nanochains. The most pronounced effects are found for Au/g-C_3N_4 and Ag/g-C_3N_4, where the light absorption strength exceeds 30 eV^{-1} and the light absorption limit is extended to 2.11 eV. It demonstrates the existence of collective plasmon excitation in the composites, that is, coherent resonance. It can be analyzed by the insets of the induced charge density distribution shown in Fig. 5. When the excitation direction is parallel to the metal nanochain, the dipole interaction between noble metal atoms appears as an attraction, which could lead to such as redshift away from the excimer resonant frequency according to the theory of dipole interaction.[34] But there are different phenomena in the higher energy region (4 eV–6 eV). Compared to the g-C_3N_4, the optical absorption of the composites decreases instead.

Furthermore, as the metal nanochains changes from Cu to Ag and then to Au, the optical absorption of the composite increases respectively, and the resonance frequency is related to the eigenfrequency of the corresponding metal nanochains. It suggests that a host–guest interaction between gCNQDs and the metal nanochains introduces a certain amount of free electrons to gCNQDs. Metal nanochains as electronic conductive channels, transfer light energy to the reaction system, thus lead to carrier concentration increase. It plays a leading role to separate photoinduced electron–hole pairs efficiently and further

enhance the visible-light photocatalytic. Pristine gCNQDs can recombine with electron-rich systems through charge-transfer complexation to form nanocomposites, resulting in a rearrangement of the electron density. Owing to composition with metal nanochains, especially gold, composites expand light absorption into the near-infrared region of g-C_3N_4 from the ultraviolet region. It does not require the high cost of pure metal but exhibits stronger light absorption, which improves its application potential in wide-light photosensitive detectors and photocatalytic.

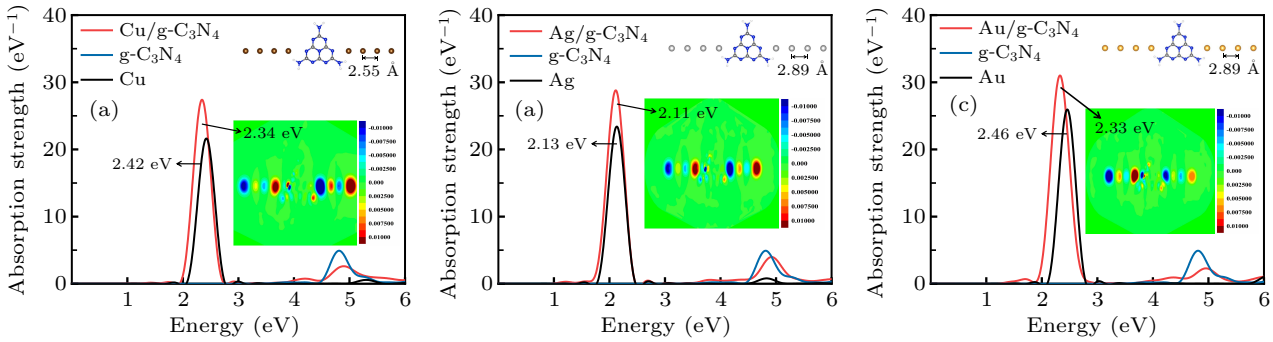


Fig. 5. Optical absorption of (a) Cu/g-C_3N_4, g-C_3N_4, Cu nanochains, (b) Ag/g-C_3N_4, g-C_3N_4, Ag nanochains, (c) Ag/g-C_3N_4, g-C_3N_4 and Au nanochains. Illustrations are Fourier transform of the induced charge density distribution of (a) Cu/g-C_3N_4 at 2.34 eV, (b) Ag/g-C_3N_4 at 2.11 eV, and (c) Au/g-C_3N_4 at 2.33 eV.

3.2.3. Functional group modification of gCNQDs

Since carbon nitride itself is metal-free, it can also tolerate functional groups. Another approach for modification of the textural structure of g-C_3N_4 is the introduction of other organic additives during the polymerization process of the nitrogen precursor. So the modified tri-s-triazine ring with specific anchoring groups may enhance its light-harvesting ability and be suitable for multipurpose applications in biosensors and biomass conversion. Schwinghammer *et al.*[35] fabricated an amorphous variant of poly (triazine imide) exhibiting an extended better hydrogen evolution activity due to light absorption up to 800 nm. We still focus on monomer gCNQDs and replace its three bridging nitrogen atoms with amino (–NH_2), hydroxyl (–OH), and methyl (–CH_3). In Fig. 6, the absorption peaks of $CNNH_2$, CNOH, and $CNCH_3$ (structures shown in Figs. 7(b)–7(d) respectively) sequentially blue shift, which is conducive to the application of deep ultraviolet photoelectric detection.

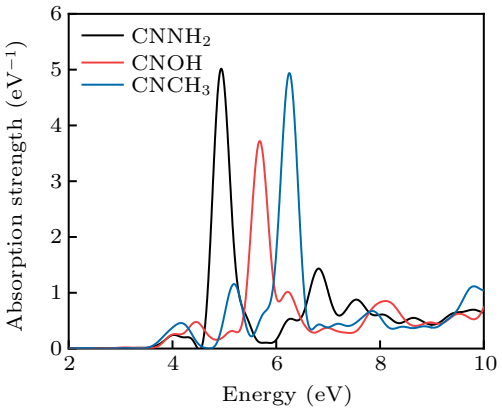


Fig. 6. Optical absorption of $CNNH_2$, CNOH, and $CNCH_3$.

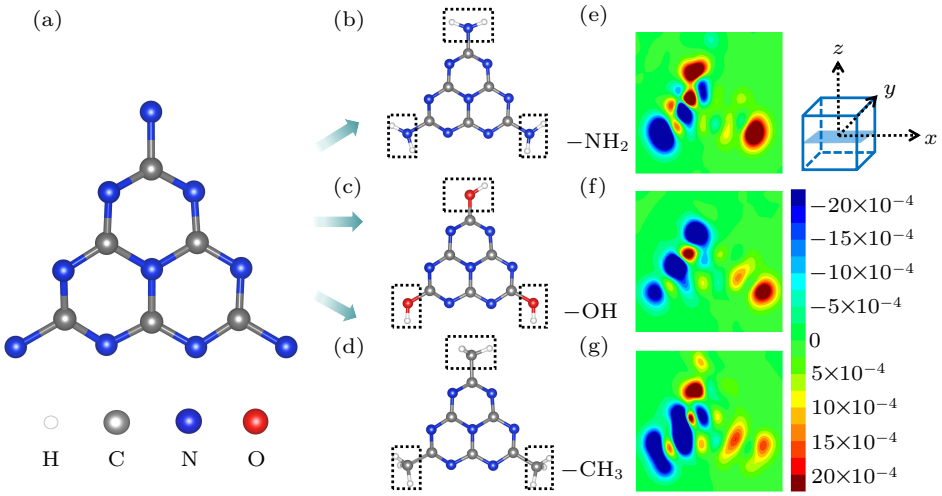


Fig. 7. (a) Structure of minimum periodic unit of monolayer g-C_3N_4 and QDs modified with amino groups ($CNNH_2$), hydroxyl groups (CNOH), and methyl groups ($CNCH_3$). Fourier transformations of induced-charge density distribution at energy resonance points for (e) $CNNH_2$, (f) CNOH, and (g) $CHCH_3$. Selected bond lengths: N–H = 1.01Å; O–H = 2.28 Å; C–H = 1.09 Å. White, silver, blue, and red atoms sand for hydrogen, carbon, nitrogen, and oxygen, respectively.

The advantages of the group to electronic modification in gCNQDs are different from those in periodic g-C_3N_4. Figures 7(e)–7(g) reveal that the reason for the difference is the change of the oscillation mode, which manifests as the electron transfer from long range to short range. Although the dipole response still exists, the electron–hole pairs gradually disperse from the structure boundary. In fact, the replacement of bridging nitrogen atoms changes the nitrogen-rich environment for the smallest gCNQDs. It is also attributed to the boundary effect on the nanometer scale, which can be observed directly with STM and scanning tunneling spectroscopy experiments.[36]

3.3. Nonlinear optical response of gCNQDs

Recently, the g-C_3N_4 QDs have been used as fluorescent probes for HeLa cell imaging.[37] Its application is extended to the fields of *in vitro* bioimaging,[38] biological analysis, and photodynamic therapy.[39,40] Increasing researches have been devoted to the nonlinear optical properties of QDs, attracting people's interest from the perspective of basic science to study various potential applications.[41,42] The external field effect is an effective tool for studying the carrier dynamics of organic semiconductors.[43,44] Herein, gCNQDs mentioned above are selected to study the change of electron occupancy state over time by calculating the highest electron level (HEL) and density of states (DOS) of QDs under the ultrafast laser. The wavelength range of the incident lasers is from 194 nm to 900 nm, covering common ultraviolet lasers to infrared lasers. Figures 8(a)–8(c) show an experimental model equipped with a linearly polarized incident laser to illuminate the waveguide and laser detector of gCNQDs.

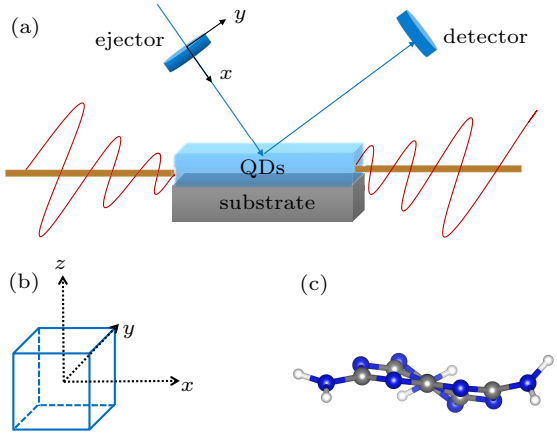


Fig. 8. (a) Schematic demonstration of proposed experimental geometry. The incident laser is emitted along (b) x direction parallel to the upper surface of (c) gCNQDs.

We explore the interaction between ultrafast laser and gCNQDs and study the time-dependent HEL under different wavelength lasers with intensities of 5 eV/Å as shown in Fig. 9(a). The ultrafast laser lasts 6 fs, but we investigate the interaction till 8 fs owing to the laser delay effect.[45] We find that HELs amplitude is significantly reduced when the laser incident time reaches 4.5 fs. HELs in final states increase first and then decrease with the decrease of the incident laser wavelength. Notably, when the wavelength decreases to 337 nm (the ultraviolet region), the HEL crosses the Fermi level unexpectedly. However, when the wavelength decreases below 337 nm, the HEL drops sharply to an insulating state.

The main reason for this phenomenon is that the 337 nm closer to the intrinsic frequency of gCNQDs allows optical carriers to obtain higher resonance energy. The shorter the laser wavelength, the higher the energy. When the energy exceeds the potential to bind the electrons, the outermost electrons are destroyed after absorbing laser energy. Therefore, the HEL exceeds the Fermi level and photoelectric conversion makes gCNQDs realize the transition to the metallic state and the state lasts to 8 fs. But in the case of wavelengths of 250 nm and 190 nm, the HEL of gCNQDs crosses the Fermi level at around 1.75 fs. A brief metallic state appears, but eventually the electronic level collapse occurs. The higher energy speeds up the electronic oscillation and brings electrons closer to the nucleus in the scattering process.[46]

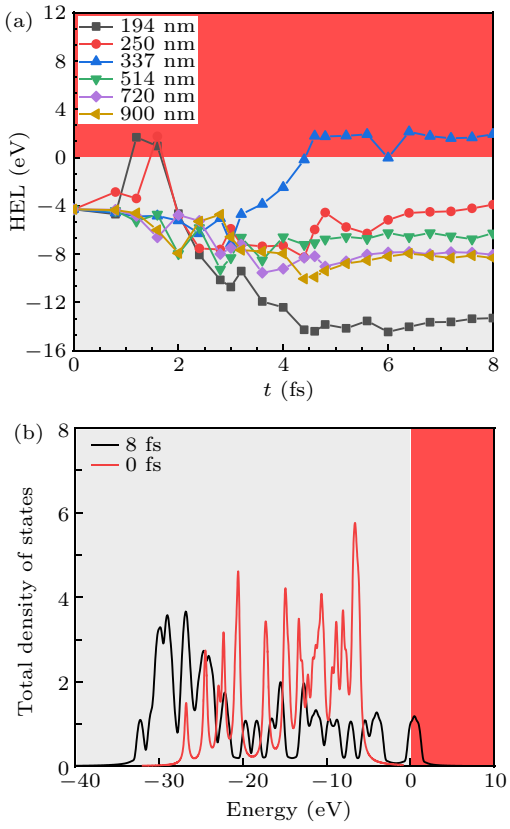


Fig. 9. (a) HEL in gCNQDs with intensity of incident ultrafast laser being 5.0 eV/Å for various wavelengths of 194 nm, 250 nm, 337 nm, 514 nm, 720 nm, and 900 nm. (b) DOS of gCNQDs at 0 fs and 9 fs with intensity of incident ultrafast laser being 5.0 eV/Å for wavelength of 337 nm.

In Fig. 9(b), the change of intrinsic DOS from the initial to final state visually shows the electronic occupied state and the electrons across the Fermi level. Electron–electron interaction can insulate conductive materials, and insulating–metal

phase transition is a typical expression of the competition between charge-carrier itinerancy and localization.[47]

To further explore the interaction of gCNQDs with the 600 nm wavelength laser, we adopt an intensity range from 4.5 eV/Å to 5.5 eV/Å with an interval of 0.25 eV/Å as shown in Fig. 10(a). The influence of the electric field intensity is non-negligible. In Fig. 10(b), the degree of HEL fluctuation increases as the electric field intensity increases and is inseparable from the laser waveform. When the laser intensity exceeds 5 eV/Å, HELs cross the Fermi level, which verifies the above phenomenon of transition to metal. It reflects from the side that, like the two-dimensional g-C_3N_4,[48] gCNQDs also exhibit excellent stability.

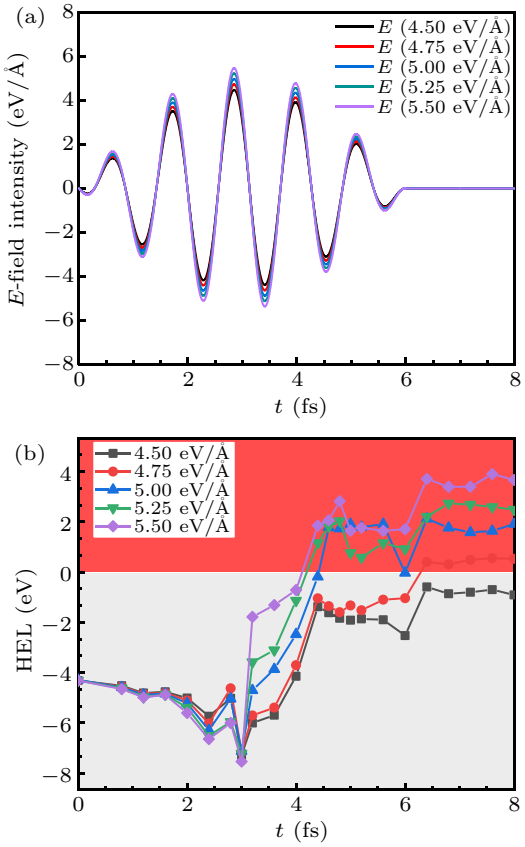


Fig. 10. (a) Laser oscillograph and (b) HEL in gCNQDs under 337 nm incident ultrafast laser with various intensities of 4.5 eV/Å, 4.75 eV/Å, 5.0 eV/Å, 5.25 eV/Å, and 5.5 eV/Å.

We explore the conditions for laser-induced changes in the structure and physical properties of gCNQDs. The critical external field condition for the transition to the metallic state is about 337 nm wavelength laser and 5 eV electric field intensity. The results laid a theoretical foundation for the experimental preparation of gCNQDs and the research in the field of laser surface modification.

4. Conclusion

We studied the linear and nonlinear optical response of gCNQDs, based on time-dependent density functional theory. Under the control of direction, the number of layers, and size, the light absorption and dipole response of each gCNQDs exhibit different characteristics, which could engineer the band gap of gCNQDs. Through the design of sophisticated gCNQDs composited with noble metal nanochains, we improved the absorption and utilization in the visible light region of gCNQDs significantly. Metal/gCNQDs composites may be used as metalloenzymes in future. For nonlinear response, gCNQDs display high stability overall. Lone pair electrons provided by it facilitate its electronic coupling with non-metal electrodes, thus making it useful in metal-free high-performance storage devices. Depending on the successful combination of theoretical prediction and experimental technique for g-C_3N_4 in the field of quantum devices, plenty of other capacities should be explored to develop commonly available materials across the areas of heterogeneous catalysis, biosensors, and nano-plasma devices. The further theoretical calculation is still on its way.

References

[1] Wen J Q, Xie J, Chen X B and Li X 2017 *Appl. Surf. Sci.* **391** 72
[2] Sun Y P, Ha W, Chen J, Qi H Y and Shi Y P 2016 *Trac-Trends Anal. Chem.* **84** 12
[3] Cao S W, Jiang J, Zhu B C and Yu J G 2016 *Phys. Chem. Chem. Phys.* **18** 19457
[4] Ke X, Yang M M, Wang W Z, Luo D X and Zhang M L 2019 *Materials* **12** 2558
[5] Zhu B C, Xia P F, Li Y H, Ho W K and Yu J G 2017 *Appl. Surf. Sci.* **391** 175
[6] Lam S M, Sin J C and Mohamed A R 2016 *Mater. Sci. Semicond. Process* **47** 62
[7] Ye S, Wang R, Wu M Z and Yuan Y P 2015 *Appl. Surf. Sci.* **358** 15
[8] Xia P F, Zhu B C, Yu J G, Cao S W and Jaroniec M 2017 *J. Mater. Chem. A* **5** 3230
[9] Li Y, Feng X H, Lu Z X, Yin H, Liu F and Xiang Q J 2018 *J. Colloid Interface Sci.* **513** 866
[10] Fu J W, Yu J G, Jiang C J and Cheng B 2018 *Adv. Energy Mater.* **8** 1701503
[11] He K L, Xie J, Liu Z Q, Li N, Chen X B, Hu J and Li X 2018 *J. Mater. Chem. A* **6** 13110
[12] Kumar S, Dhiman A, Sudhagar P and Krishnan V 2018 *Appl. Surf. Sci.* **447** 802
[13] Wang Y, Wang X C and Antonietti M 2012 *Angew. Chem. Int. Ed.* **51** 68
[14] Zheng Y, Liu J, Liang J, Jaroniec M and Qiao S Z 2012 *Energy Environ. Sci.* **5** 6717
[15] Yang S B, Gong Y J, Zhang J S, Zhan L, Ma L L, Fang Z Y, Vajtai R, Wang X C and Ajayan P M 2013 *Adv. Mater.* **25** 2452
[16] Zhang J S, Chen Y and Wang X C 2015 *Energy Environ. Sci.* **8** 3092
[17] Sun S D and Liang S H 2017 *Nanoscale* **9** 10544
[18] Wang W J, Jimmy C Y, Shen Z R, Chan D K L and Gu T 2014 *Chem. Commun.* **50** 10148
[19] Sano T, Tsutsui S, Koike K, Hirakawa T, Teramoto Y, Negishi N and Takeuchi K 2013 *J. Mater. Chem. A* **1** 6489
[20] Zhang J S, Guo F S and Wang X C 2013 *Adv. Funct. Mater.* **23** 3008
[21] Segall M D, Lindan P L D, Probert M J, Pickard C J, Hasnip P J, Clark S J and Payne M C 2002 *J. Phys.: Condens. Matter* **14** 2717
[22] Marques M A, Castro A, Bertsch G F and Rubio A 2003 *Comput. Phys. Commun.* **151** 60
[23] Perdew J P, Chevary J A, Vosko S H, Jackson K A, Pederson M R, Singh D J and Fiolhais C 1992 *Phys. Rev. B* **46** 6671
[24] Onida G, Reining L and Rubio A 2002 *Rev. Mod. Phys.* **74** 601
[25] Botti S, Schindlmayr A, Del Sole R and Reining L 2007 *Rep. Prog. Phys.* **70** 357
[26] Li Y, Li X, Zhang H W, Fan J J and Xiang Q J 2020 *J. Mater. Sci. Technol.* **56** 69

[27] Huang Q, Yu J G, Cao S W, Cui C and Cheng B 2015 *Appl. Surf. Sci.* **358** 350
[28] Prodan E, Radloff C, Halas N J and Nordlander P 2003 *Science* **302** 419
[29] Yan J, Yuan Z and Gao S W 2007 *Phys. Rev. Lett.* **98** 216602
[30] Yan J and Gao S W 2008 *Phys. Rev. B* **78** 235413
[31] Zhao F, Cheng H H, Hu Y, Song L, Zhang Z P, Jiang L and Qu L T 2014 *Sci. Rep.* **4** 5882
[32] Cheng Q, He Y, Ge Y L, Zhou J G and Song G W 2018 *Microchim. Acta* **185** 332
[33] Nilius N, Wallis T M and Ho W 2002 *Science* **297** 1853
[34] Mishchenko E G, Shytov A V and Silvestrov P G 2010 *Phys. Rev. Lett.* **104** 156806
[35] Schwinghammer K, Tuffy B, Mesch M B, Wirnhier E, Martineau C, Taulelle F, Schnick W, Senker J and Lotsch B V 2013 *Angew. Chem. Int. Ed.* **52** 2435
[36] Kobayashi Y, Fukui K I, Enoki T, Kusakabe K and Kaburagi Y 2005 *Phys. Rev. B* **71** 193406
[37] Li H, Shao F Q, Huang H, Feng J J and Wang A J 2016 *Sens. Actuators B Chem.* **226** 506
[38] Zhan Y, Liu Z M, Liu Q Q, Huang D, Wei Y, Hu Y C, Lian X J and Hu C F 2017 *New J. Chem.* **41** 3930
[39] Chan M H, Chen C W, Lee I J, Chan Y C, Tu D T, Hsiao M, Chen C H, Chen X Y and Liu R S 2016 *Inorg. Chem.* **55** 10267
[40] Chan M H, Pan Y T, Lee I J, Chen C W, Chan Y C, Hsiao M, Wang F, Sun L D, Chen X Y and Liu R S 2017 *Small* **13** 1700038
[41] Autere A, Jussila H, Dai Y Y, Wang Y D, Lipsanen H and Sun Z P 2018 *Adv. Mater.* **30** 1705963
[42] Cavalleri A 2018 *Science* **362** 525
[43] Zhang C, Sun D, Sheng C X, Zhai Y X, Mielczarek K, Zakhidov A and Vardeny Z V 2015 *Nat. Phys.* **11** 427
[44] Fan M Q, Li T, Li G Q, Zhao S Z, Yang K J, Zhang S Y, Zhang B T, Xu J Q and Krankel C 2017 *Opt. Express* **25** 12796
[45] Anisimov S I, Kapeliovich B L and Perelman T L 1974 *Sov. Phys. JETP* **39** 375
[46] Lin J H, Zhang H, Zhang B F, Zhao J M, Miyamoto Y and Cheng X L 2018 *J. Phys. Chem. C* **122** 19992
[47] Liu M K, Hwang H Y, Tao H, Strikwerda A C, Fan K, Keiser G R, Sternbach A J, West K G, Kittiwatanakul S, Lu J W, Wolf S A, Omenetto F G, Zhang X, Nelson K A and Averitt R D 2012 *Nature* **487** 345
[48] Tian N, Huang H W, Du X, Dong F and Zhang Y H 2019 *J. Mater. Chem. A* **7** 11584